Energy & Environmental Science

Cite this: *Energy Environ. Sci.*, 2011, **4**, 2894

www.rsc.org/ees

PAPER

All-conjugated poly(3-alkylthiophene) diblock copolymer-based bulk heterojunction solar cells with controlled molecular organization and nanoscale morphology†

Ming He,[ab] Wei Han,[ac] Jing Ge,[b] Yuliang Yang,[b] Feng Qiu*[b] and Zhiqun Lin*[ac]

Received 20th April 2011, Accepted 17th May 2011
DOI: 10.1039/c1ee01509e

Control over the ratio of two blocks in *a new class of all-conjugated diblock copolymers*, poly-(3-butylthiophene)-*b*-poly(3-hexylthiophene) (P3BHT), provides a facile approach to precisely tune the molecular organization and nanoscale morphology in polymer bulk heterojunction (BHJ) solar cells. In stark contrast to the power conversion efficiency, PCE, of 1.08% in poly(3-butylthiophene) (P3BT)/[6,6]-phenyl-C_{71}-butyric acid methyl ester ($PC_{71}BM$) and 3.54% in poly(3-hexylthiophene) (P3HT)/$PC_{71}BM$ solar cells, an attractive, high PCE of 4.02% was achieved in a P3BHT21/$PC_{71}BM$ BHJ device in which the molar ratio of P3BT : P3HT in P3BHT21 was 2 : 1. The ratio of P3BT and P3HT blocks was found to exert a noteworthy influence on the molecular organization of P3BHT, the film morphology of P3BHT/$PC_{71}BM$ blend, and the final performance of P3BHT/$PC_{71}BM$ photovoltaic devices. This enhanced performance reflected a synergy of finer phase separation of P3BHT21 and $PC_{71}BM$ and the formation of respective percolation networks of electron donor P3BHT and electron acceptor $PC_{71}BM$. The P3HT block rendered the P3BHT chains with favorable chemical compatibility for the diffusion of $PC_{71}BM$ molecules, allowing for finer phase separation between P3BHT crystalline domains and $PC_{71}BM$ domains at the nanoscale and maximizing the interfacial area of P3BHT21/$PC_{71}BM$ for improved charge generation. The P3BT block facilitated the self-assembly of P3BHT chains into sufficient interpenetrating pathways for efficient charge transport and collection. Moreover, a small crystalline domain with a size of 10.4 nm formed in the active layer that is comparable to the exciton diffusion length of most conjugated polymers (~10 nm).

[a]*Department of Materials Science and Engineering, Iowa State University, Ames, IA, 50010, USA. E-mail: zhiqun.lin@mse.gatech.edu; Fax: +1 515-294-7202; Tel: +1 515-294-9967*
[b]*The Key Laboratory of Molecular Engineering of Polymers, Ministry of Education, Department of Macromolecular Science, Fudan University, Shanghai, 200433, China. E-mail: fengqiu@fudan.edu.cn*
[c]*School of Materials Science and Engineering, Georgia Institute of Technology, Atlanta, GA, 30332, USA*

† Electronic supplementary information (ESI) available: AFM height images of blend films and parameters extracted from SCLC curves. See DOI: 10.1039/c1ee01509e

Broader context

The polymer bulk heterojunction (BHJ) solar cell is widely recognized as one of the most promising approaches for producing lightweight, flexible, low-cost devices to harvest solar energy. Extensive efforts have been devoted to optimizing the molecular organization, improving the film morphology, and thus promoting the photovoltaic performance. The merit of designing P3BHT diblock copolymers in the present study is to incorporate poly(3-alkylthiophenes) with different alkyl side chains to balance and optimize the solubility, molecular organization, phase separation with $PC_{71}BM$ molecules, and thus the electronic and optoelectronic properties. We achieved not only the highest charge mobility in such co-crystalline P3BHT phases for effective charge transport, but also polythiophene crystalline domain in the size of 10.4 nm (compared with those of 14.4 nm in P3HT and 22.7 nm in P3BT homopolymers) for efficient charge generation as P3BHT domain size is commensurate with the diffusion length of photogenerated excitons in polymers. The strategy of precisely controlling the ratio of the blocks in an all-conjugated block copolymer to yield improved photovoltaic performance may provide insight into many aspects of solar energy conversion, from rational design and synthesis of new materials to engineering of high-efficiency polymer BHJ solar cells.

1. Introduction

Bulk heterojunctions (BHJs) have been widely recognized as an attractive approach for improving the efficiency of polymer-based photovoltaics, which hold promise for low-cost, light-weight, roll-to-roll production of large-area flexible devices for commercial applications.[1] The power conversion efficiency (PCE) of polymer BHJ solar cells depends heavily on the energy level of the donor and acceptor materials as well as the film morphology of active layers. A well-matched energy level offset between the highest occupied molecular orbital (HOMO) of the donor and the lowest unoccupied molecular orbital (LUMO) of the acceptor maximizes the open-circuit voltage (V_{oc}). On the other hand, a fine scale of phase separation within the exciton (*i.e.*, the electron–hole pair) diffusion range and with bicontinuous pathways for transport of charge carriers to the electrodes maximizes the short circuit current density (J_{sc}) and the fill factor (FF).[2] Over the past several years, a significant improvement in PCE has been achieved *via* innovative design and synthesis of new donor and acceptor materials and the optimization of the nanoscale morphology of active layers.[3–8] The highest PCE of 7.4% using benzodithiophene polymers blended with [6,6]-phenyl-C_{71}-butyric acid methyl ester ($PC_{71}BM$) has recently been reported.[9] In conjunction with the experimental studies, computer simulation has predicted that, upon designing new donor and acceptor materials with small exciton binding energy, balancing the HOMO and LUMO levels of donor and acceptor materials, respectively, forming better interpenetrating networks within the entire photoactive layer, and improving charge collection at the active layer/electrode interface, the attainable PCE of polymer BHJ solar cells could reach 10% for single cells and 15% for tandem cells.[2,10,11]

One of the most widely studied polymer BHJ solar cells utilizes the conjugated polymer, poly(3-hexylthiophene) (P3HT) as the electron donor and a fullerene derivative (*e.g.*, [6,6]-phenyl-C_{61}-butyric acid methyl ester (PCBM)) as the electron acceptor. P3HT self-organizes into semicrystalline structures involving lamellar packing of π-stacked thienyl backbones separated by layers of hexyl side chains.[12] The performance of P3HT/PCBM solar cells is highly correlated with the ordered arrangement of P3HT chains within the active layer (*i.e.*, forming crystalline order), which enhances the light absorption and improves the hole mobility and charge transport.[13] Additionally, the morphology of the P3HT/PCBM film greatly influences the efficiency of charge generation *via* nanoscale phase separation that leads to a large interfacial area between the two components, as well as the efficiency of charge transport *via* the development of percolation networks spanning the thickness of the device.[14]

Considerable efforts on improving the nanoscale alignment of P3HT chains (*i.e.*, crystallization) have been made, including the application of thermal annealing[15,16] and solvent annealing,[17–20] the use of additive,[21] and the construction of inverted device configurations,[22–26] thereby resulting in optimized molecular organizations of P3HT and film morphologies having reproducible 3–5% PCE. Notably, alteration of the length of side chains of poly(3-alkylthiophene)s (P3ATs) to less or more than hexyl alkane was found to lead to a marked decrease in opto-electronic performance, which is indicative of the strong influence of alkyl side chains as solubilizing substituents on the interfacial interactions between P3ATs and PCBM. The solubility, self-assembly, charge intensity, electronic energy level, and absorption coefficient of P3ATs vary with different length of side chains.[27] Of particular interest is poly(3-butylthiophene) (P3BT), which exhibits an extraordinarily high hole mobility of 1×10^{-3} cm^2 V^{-1} s^{-1} in the P3BT-nanowires/PCBM blend film due to intense stacking of thienyl chains with short butyl side chains.[28]

Recent advances in synthesis techniques render the design of functional all-conjugated block copolymers composed of two dissimilar rod-like blocks covalently linked at one end, which may spontaneously phase separate into ordered, controllable structures on the 10 nm length scale comparable to the exciton diffusion length of the conjugated polymer, and provide optimized morphologies for charge generation and transport.[29] Compared to P3AT homopolymers, a rational control over the formation of large-area ordered nanostructure and attractive electronic activity may be realized with the P3AT-based all-conjugated diblock copolymer by judiciously controlling the compositions of two alkyl side chains in the diblock copolymer (*i.e.*, different length of alkyl substituents), leading to completely different solubilities and stacking of polymer chains from the homopolymer counterparts.[12] As such, the synthesis and self-assembly of such rod–rod diblock copolymers that possess both intriguing nanostructures and electronic activities provide expanded opportunities for developing high-performance polymer BHJ solar cells. However, due primarily to the rigid nature of rod-like polymer chains which complicates the synthesis and their self-assembly, the physical properties and self-assembly mechanism of these rod–rod diblock copolymers are far less understood than those of widely studied coil–coil and rod–coil diblock copolymers.[12]

Herein, we report, *for the first time*, the molecular organization of *a new class of all-conjugated diblock copolymers*, poly-(3-butylthiophene)-*b*-poly(3-hexylthiophene) (P3BHT) chains (*i.e.*, the packing of interchains), and the nanoscale morphology of the resulting P3BHT/$PC_{71}BM$ thin blend films, which can be precisely controlled by tailoring the molar ratio of P3BT and P3HT blocks in P3BHT, thereby leading to solar cells with improved performance. In contrast to the PCE of 1.08% in P3BT and 3.54% in P3HT homopolymer-based BHJ solar cells, an attractive PCE of 4.02% was achieved in a P3BHT21/$PC_{71}BM$ solar cell, in which the molar ratio of P3BT : P3HT in P3BHT21 is 2 : 1. The rod-like P3BT and P3HT blocks preferred to co-crystallize into lamellar stacking with interdigitation of butyl and hexyl chains, and the co-crystalline P3BHT domains microphase separate with $PC_{71}BM$ domains to form donor/acceptor interfaces for charge generation. The merit of designing P3BHT diblock copolymers is to incorporate poly(3-alkylthiophene)s with different alkyl side chains to balance and optimize the solubility, molecular organization, phase separation with $PC_{71}BM$ molecules, and thus the electronic and optoelectronic properties. It is expected that the P3HT block rendered the P3BHT21 chains with favorable chemical compatibility for the diffusion of $PC_{71}BM$ in the blend to form finer phase separation at the nanoscale with the maximum interfacial area of P3BHT21/$PC_{71}BM$ for charge generation, while the P3BT block with short side chains promotes the polymer chains to self-assemble into sufficient bicontinuous crystalline domains spanning the thickness of the device to maximize the charge transport and

collection. As such, the interplay of finer phase separation of P3BHT21/$PC_{71}BM$ for charge generation and the formation of interpenetrating percolation networks of P3BHT21 and $PC_{71}BM$ for charge transport and collection resulted in better optimized BHJ nanostructures, and thus a markedly improved photovoltaic performance as compared to their homopolymer counterparts.

2. Experimental section

2.1 Materials

Regioregular P3BT homopolymer (M_n = 22 400 g mol^{-1}, PDI = 1.3) and P3HT homopolymer (M_n = 19 000 g mol^{-1}, PDI = 1.2) were synthesized by a modified Grignard metathesis procedure.[30] Three P3BHT diblock copolymers, *i.e.*, P3BHT21 (P3BT : P3HT = 2 : 1 mol/mol; M_n = 8300 g mol^{-1}, PDI = 1.3), P3BHT11 (P3BT : P3HT = 1 : 1 mol/mol; M_n = 11 400 g mol^{-1}, PDI = 1.3) and P3BHT12 (P3BT : P3HT = 1 : 2 mol/mol; M_n = 15 100 g mol^{-1}, PDI = 1.3), were synthesized by a modified quasi-living chain growth polymerization.[29] The detailed synthesis can be found in our previous work.[31,32] $PC_{71}BM$ (purity > 99.5%) was purchased from American Dye Source, Inc. Poly(3,4-ethylenedioxythiophene):poly(styrene sulfonate) (PEDOT:PSS) (1.3 wt% dispersion in water, conductive grade) and anhydrous 1,2-dichlorobenzene (ODCB) were purchased from Sigma-Aldrich. Indium Tin Oxide (ITO) coated glass substrates (10 Ω $\square^{-1}$) were purchased from Delta Technologies, Ltd.

2.2 Device fabrication

The ITO-coated glass substrate was cleaned sequentially by ultrasonication in acetone, methanol and isopropanol, followed by O_2-plasma exposure for 5 min. PEDOT:PSS aqueous solution was purified with a 0.45 μm PTFE filter, and then spin-coated on the ITO substrate at 4000 rpm for 60 s and dried in a vacuum oven at 120 °C for 1 h. The thickness of the PEDOT:PSS layer was approximately 40 nm.

All devices were fabricated in a glove box filled with Ar. 50 mg ml^{-1} $PC_{71}BM$ ODCB solution was prepared by ultrasonic mixing for 1 h, and purified with a 0.45 μm PTFE filter prior to use. P3BHT was dissolved in ODCB at 90 °C to yield a 20 mg ml^{-1} P3BHT ODCB solution. The hot solution was quickly purified with a 0.45 μm PTFE filter before cooling down to room temperature. Subsequently, the P3BHT and $PC_{71}BM$ ODCB solutions at the 1 : 0.75 w/w ratio were thoroughly mixed, and spin-coated on the PEDOT:PSS surface at 1100 rpm for 40 s, followed by thermal annealing at 140 °C for 20 min. A cathode was prepared by sequentially depositing 50 nm Ca and 100 nm Al through a shadow mask onto the P3BHT/$PC_{71}BM$ active layer with a thermal evaporator at a vacuum of 2×10^{-6} torr. P3BT and P3HT homopolymer-based devices were prepared in the same way, except that the concentration of P3BT ODCB solution was 8 mg ml^{-1} due to the low solubility of P3BT in ODCB. The thicknesses of all resulting active layers used in the study were approximately 200 nm as measured by atomic force microscopy (AFM).

Devices for the space-charge limited current (SCLC) mobility measurements were fabricated in an identical manner, except that a layer of 100 nm gold was deposited on the P3BHT/$PC_{71}BM$ thin film instead of the Ca/Al layer to produce hole-only devices.

2.3 Characterization

Photovoltaic devices with an area of 0.10 ± 0.01 cm^2 were tested under simulated AM 1.5 G irradiation (100 mW cm^{-2}, calibrated with Daystar Meter) using a SoLux Solar Simulator, and the current–voltage (*I–V*) curves were measured using a Keithley 2400 multisource meter. The measurements of the SCLC *I–V* curves were also performed using the Keithley 2400 multisource meter in the dark. X-Ray diffraction (XRD) data were collected by a PANalytical X'Pert PRO X-ray diffractometer using Cu Kα_1 radiation (λ = 1.541 Å) operated at 40 kV and 40 mA. UV-Vis absorption spectra were recorded with a Newport OSM-100-UV/vis optical spectrometer. External quantum efficiencies (EQEs) were measured using an Oriel Cornerstone 130 1/8 m monochromator, and the incident light intensity was monitored by a Thorlabs Console for the Digital Optical Power Meter with a standard photodiode sensor. EQE measurements were directly conducted on the photovoltaic devices. The surface morphology of P3BHT/$PC_{71}BM$ was obtained by AFM in tapping mode (Dimension 3100 scanning force microscope; Digital Instruments). Notably, the films used for XRD, UV-Vis spectrometer and AFM measurements were prepared in an identical manner as those of photovoltaic devices, but with no Ca/Al deposited on the top.

3. Results and discussion

3.1. Self-assembly of P3BHT block copolymers

In our previous work, we demonstrated that the self-assembly of P3BHT diblock copolymers experienced different kinetic pathways from those of the P3BT and P3HT homopolymers. P3BHT diblock copolymers self-assembled into nanostructured morphologies in mixed selective solvents of anisole/chloroform.[33] A balance between the chain flexibility and crystallization may be realized in P3BHT block copolymers by judiciously controlling the volume fraction of P3BT and P3HT blocks (*i.e.*, the different length of alkyl substituents as shown in Fig. 1a), leading to completely different solubilities and stacking of polymer chains from their homopolymer counterparts.[31] Fig. 1b shows the XRD profiles of P3BHT21, P3BHT11 and P3BHT12 films prepared from their 1,2-dichlorobenzene (ODCB) solutions, all of which exhibited a single [100] peak at 2θ = 6.5°, 6.1°, and 5.8°, respectively, indicating that there was only one type of crystalline domain present in the system. Compared with the XRD profiles of P3BT and P3HT homopolymers, which showed a single [100] peak at 2θ = 7.2° and 5.7°, respectively,[31,34] it is clearly evident that P3BHT diblock copolymers with different length of alkyl side chains (*i.e.*, butyl and hexyl) co-crystallized in the blend films. The P3BT and P3HT blocks co-crystallized into a lamellar packing with the interdigitation of butyl and hexyl side chains with one another,[35] adopting the edge-on orientation with the thienyl backbone aligned parallel to the substrate as depicted in Fig. 1c. It is worth noting that with an increased composition of P3BT block, the interchain distance, d_{100}, of P3BHT12, P3BHT11, P3BHT21 progressively decreased from $d_{100,\ P3BHT12}$ = 15.0 Å to $d_{100,\ P3BHT11}$ = 14.1 Å, to $d_{100,\ P3BHT21}$ = 13.2 Å. The

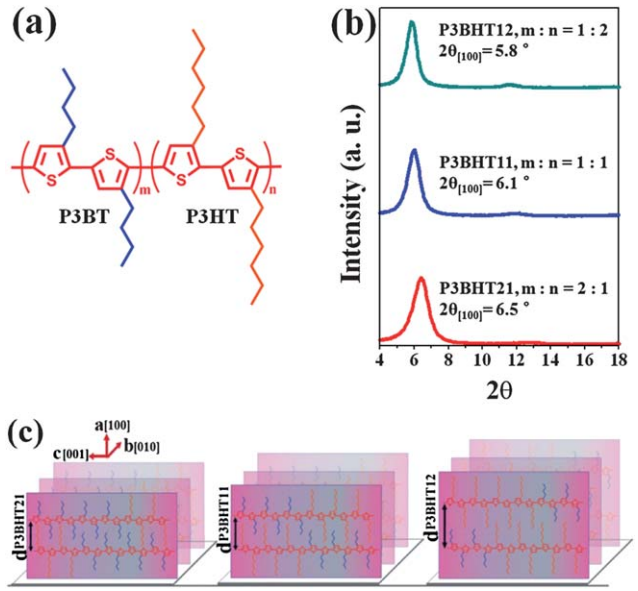

Fig. 1 (a) The chemical structure of poly(3-butylthiophene)-*b*-poly(3-hexylthiophene) (P3BHT) diblock copolymer. (b) XRD profiles of P3BHT films prepared from the P3BHT ODCB solutions. The diblock copolymers with different length of alkyl side chains used in the study were P3BHT21 (P3BT : P3HT = 2 : 1, mol/mol), P3BHT11 (P3BT : P3HT = 1 : 1, mol/mol), and P3BHT12 (P3BT : P3HT = 1 : 2, mol/mol). (c) Schematic representation of P3BHT21 (left panel), P3BHT11 (central panel), and P3BHT12 (right panel) lamella packing with the edge-on orientation. P3BHT diblock copolymers with different alkyl chain lengths tend to co-crystallize forming a crystalline lamella by interdigitating two different side chains one another with tunable interchain distance along the (100) axis (*i.e.*, side-chain direction).

incorporation of more P3BT blocks in diblock copolymers facilitated closer packing of thienyl backbones, which could be favorable to increase the charge mobility due to decreased intermolecular hopping distance along the [100] direction.[36] Hence, the combination of ordered co-crystalline P3BHT domains, tunable interchain packing and good chemical compatibility for the diffusion of $PC_{71}BM$ will offer expanded adaptability for pursuing high-performance polymer BHJ architectures.

3.2. Characteristics of P3BHT/$PC_{71}BM$ BHJ solar cells

The photovoltaic performances of P3BHT/$PC_{71}BM$ blend films were systematically investigated. The devices with the configuration of ITO/PEDOT:PSS/P3BHT:$PC_{71}BM$/Ca/Al were fabricated with P3BHT : $PC_{71}BM$ = 1 : 0.75 w/w. The P3BT/$PC_{71}BM$ and P3HT/$PC_{71}BM$ photovoltaic devices were also prepared in the same way and used as controls to assess the influence of the ratio of two blocks in P3BHT on the device performance (see *Experimental*). Fig. 2 shows the current density–voltage (*J*–*V*) curves of P3BT/$PC_{71}BM$, P3BHT/$PC_{71}BM$, and P3HT/$PC_{71}BM$ photovoltaic devices under AM 1.5 G illumination (100 mW cm^{-2}). The photovoltaic performances were summarized in Table 1. Consistent with those previously reported, the P3HT/$PC_{71}BM$ device exhibited a much higher PCE of 3.54% than 1.08% in the P3BT/$PC_{71}BM$ device. This was attributed to the presence of a hexyl side chain that is capable of achieving a homogeneous phase separation of P3HT and $PC_{71}BM$ in conjunction with a dense network of P3HT crystalline domains throughout the blend film.[37] Despite the fact that the hole mobility of P3AT generally increases with the decrease in the length of alkyl side chains, the performance of the P3BT/$PC_{71}BM$ photovoltaic device suffered from low V_{oc} and FF as the longer side chain was required to facilitate the diffusion of PCBM and phase separation in the blend film.[38] Quite intriguingly, for P3BHT diblock copolymers, more P3BT blocks in the copolymers appeared to yield improved performance (Fig. 2a and Table 1), clearly indicating that a delicate balance between the chain flexibility and self-assembly can be readily established by adjusting the ratio of alkyl side chains, which in turn led to the optimization of phase separation between P3BHT and $PC_{71}BM$ for charge generation and continuous pathways for charge transport.

As the composition of P3BT block in P3BHT reduced, the J_{sc} dropped slightly from 10.3 mA cm^{-2} in P3BHT21/$PC_{71}BM$ to 9.95 mA cm^{-2} in P3BHT11/$PC_{71}BM$, and significantly to 4.55 mA cm^{-2} in P3BHT12/$PC_{71}BM$ (Table 1). The FF decreased

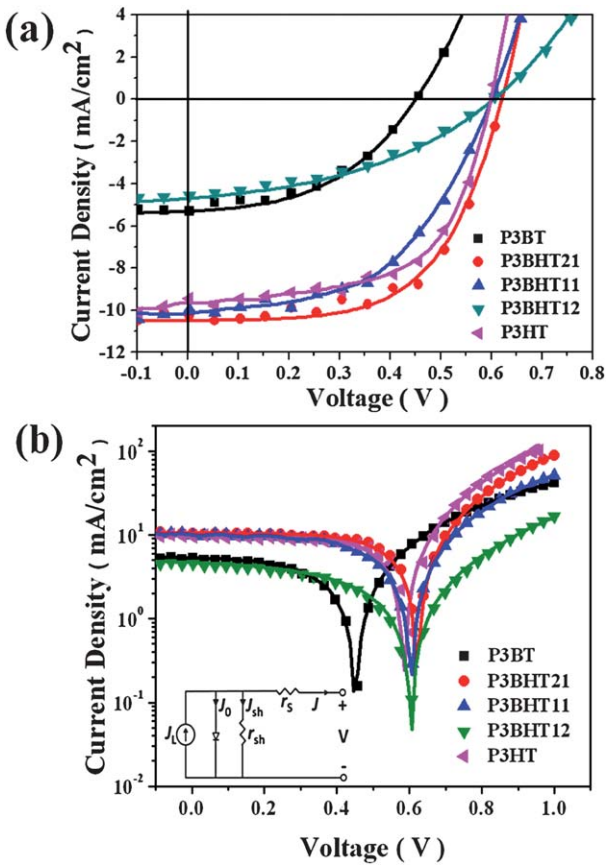

Fig. 2 (a) *J*–*V* curves of bulk heterojunction solar cells fabricated from P3BT/$PC_{71}BM$, P3BHT/$PC_{71}BM$, and P3HT/$PC_{71}BM$ solar cells under AM 1.5 G illumination at 100 mW cm^{-2}. The P3BHT diblock copolymers used were P3BHT21 (P3BT : P3HT = 2 : 1, mol/mol), P3BHT11 (P3BT : P3HT = 1 : 1, mol/mol), and P3BHT12 (P3BT : P3HT = 1 : 2, mol/mol). (b) Single diode fits to the *J*–*V* curves of P3BT/$PC_{71}BM$, P3BHT/$PC_{71}BM$, and P3HT/$PC_{71}BM$ solar cells, in which the symbols are experimental data, and the solid lines are the corresponding theoretical fits. The single diode model is depicted in the inset.

Table 1 Summary of photovoltaic performances of P3BT/$PC_{71}BM$, P3BHT/$PC_{71}BM$, and P3HT/$PC_{71}BM$ solar cells under AM 1.5 G illumination at 100 mW cm^{-2}

P3BHT:$PC_{71}BM$	V_{oc}/V	J_{sc}/mA cm^{-2}	FF (%)	PCE (%)
P3BT	0.46	5.30	44.5	1.08
P3BHT21	0.63	10.3	62.1	4.02
P3BHT11	0.61	9.95	52.7	3.18
P3BHT12	0.61	4.55	40.9	1.13
P3HT	0.61	9.43	61.8	3.54

from 62.1% in P3BHT21/$PC_{71}BM$ to 52.7% in P3BHT11/$PC_{71}BM$, and to 40.9% in P3BHT12/$PC_{71}BM$. Consequently, the PCEs dropped. The decrease in J_{sc} and FF with less P3BT blocks incorporated in P3BHT can be regarded as an important signature of large scale phase separation and/or reduced degree of crystallinity of P3BHT in the blend films.[2] Taken together with a recent study on poly(3-butylthiophene)-*b*-poly(3-octylthiophene) (P3BOT) based devices (*i.e.*, P3BOT/$PC_{71}BM$), in which a highest PCE of 3.0% was achieved at 50 mol% P3BT block in P3BOT,[27] it is clear that the performance of all-conjugated P3AT diblock copolymer-based devices depends on not only the ratio of two blocks but also the length of alkyl side chains in the copolymers, signifying that the variation in the alkyl substituent could profoundly impact the solubility and structural order of polymer chains, and thus critically affecting the resulting device performance.[39]

It is noteworthy that the P3BHT21/$PC_{71}BM$ photovoltaic device possessed an impressive PCE of 4.02%. To the best of our knowledge, this is the highest efficiency among rod–rod diblock copolymer based BHJ solar cells reported, even higher than that of the P3HT/$PC_{71}BM$ solar cell prepared under the same conditions in the present study (PCE = 3.54%), thereby offering an avenue in developing high-efficiency solar cells. We note that the present study primarily focused on the molecular design of novel all-conjugated diblock copolymers to produce high-performance devices, and the device-fabricating condition for P3BHT/$PC_{71}BM$ solar cells followed the optimized condition for preparing P3HT/$PC_{71}BM$ solar cells.[2] Further improvement of performance in the P3BHT21-based photovoltaics is expected as there remains room for optimization of many parameters of the device assembly, including P3BHT molecular weight, film thickness, P3BHT/$PC_{71}BM$ mixing ratio, device annealing conditions (*e.g.*, thermal annealing, solvent vapor annealing), *etc.*

We now turn our attention to qualitatively understand the photophysical behavior of P3BHT-based devices and elucidate the origin of varied performance of devices with different ratio of P3BT and P3HT blocks in P3BHT. The *J*–*V* characteristics of P3BT/$PC_{71}BM$, P3HT/$PC_{71}BM$, and P3BHT/$PC_{71}BM$ devices were fitted into an electrically equivalent single diode model (inset in Fig. 2b):[40]

$$J = J_L - J_0\left\{\exp\left[\frac{q(V + Jr_s)}{nkT}\right] - 1\right\} - \frac{V + Jr_s}{r_{sh}} \quad (1)$$

where J is the current density, V is the applied voltage, J_L is the photogenerated current density, J_0 is the reverse saturation current density, r_s is the specific series resistance, r_{sh} is the specific shunt resistance, n is the diode ideality factor ($n = 1$ for an ideal diode), q is the elementary charge, k is the Boltzmann's constant, and T is the absolute temperature. The parameters J_L, J_0, n, r_s and r_{sh} can be extracted from the nonlinear least-square fits to the photovoltaic *J*–*V* curves. The fitting agreed very well with the experimental results as shown in Fig. 1b. The fitting parameters are summarized in Table 2. In polymer BHJ solar cells, the semiconductor donor and acceptor components are required to phase separate into small domains to create a large interface for efficient exciton diffusion and charge generation, as typical exciton diffusion length in the conjugated polymer is limited to 10 nm.[41] On the other hand, the charge transport largely depends on the film morphology of the active layer, in which both the donor and acceptor phases should form nanoscale interpenetrating networks within the whole active layer to ensure an efficient charge transport to electrodes.[1] Based on the analysis of the single diode model, the photogenerated current density J_L qualitatively reflects the efficiency of exciton diffusion and charge generation in the device (Table 2).[42] The fact that the P3BHT21-, P3BHT11- and P3HT-based devices showed similarly high J_L around 10 mA cm^{-2}, suggested that the exciton efficiently diffused and the charge was created in the blends without striking recombination. In contrast, the much lower J_L in P3BHT12- and P3BT-based devices implied that there may exist a large size of donor and acceptor domains and/or limited donor/acceptor phase separation in the blend films.[41]

According to traditional diode theory, the ideality factor n describes how closely the behavior of a diode matches an ideal diode in which no recombination occurs ($n = 1$). In polymer BHJ solar cells, n is suggested to be characteristic of the recombination behavior in the blend film, and thus a change in n provides evidence that there may be a different type of mechanism for the recombination loss.[43–45] The reverse saturation current density J_0 is a measure of the carrier leakage in the vicinity of the barrier caused by recombination, which is at the donor/acceptor interface in polymer BHJ solar cells.[45] The highest n and J_0 in P3BHT12 indicated that strong charge recombination occurred at the P3BHT12/$PC_{71}BM$ interface, thereby leading to diminished charge generation and charge transport. This also explained the low performance in the P3BT/$PC_{71}BM$ device. In stark contrast, the pronounced performance in P3BHT21/$PC_{71}BM$ stemmed from an optimized combination of fitted parameters (Table 2), namely, the lowest reverse saturation current density J_0, the smallest ideality factor n, the decreased series r_s, and the large shunt resistance r_{sh}, revealing that the film morphology with the least recombination loss for charge generation and transport was achieved.

3.3. Morphology of P3BHT/$PC_{71}BM$ blend films

To verify the analyses described above, the film morphology and the molecular organization of the blend films were scrutinized. Fig. 3 shows AFM phase images of the P3BT/$PC_{71}BM$, P3BHT/$PC_{71}BM$, and P3HT/$PC_{71}BM$ blend films. The crystalline P3AT homopolymers (or diblock copolymers) appeared bright while $PC_{71}BM$ appeared dark in the phase images.[36] Typically, the P3HT/$PC_{71}BM$ blend film exhibited nanoscale phase separation composed of grain-like P3HT crystalline domains and P3HT amorphous domains with $PC_{71}BM$ situated (*i.e.*, $PC_{71}BM$ domains) as shown in Fig. 3e.In contrast, more densely interconnected crystalline domains emerged in the

Table 2 Summary of photovoltaic parameters extracted from the *J–V* curves of P3BT/$PC_{71}BM$, P3BHT/$PC_{71}BM$, and P3HT/$PC_{71}BM$ solar cells using the single diode model

P3BHT:$PC_{71}BM$	J_L/mA cm^{-2}	J_0/mA cm^{-2}	n	r_s/Ω cm^2	r_{sh}/Ω cm^2	PCE (%)
P3BT	5.4	0.109	4.44	7.13	1.15×10^3	1.08
P3BHT21	10.5	0.014	3.61	1.91	1.42×10^3	4.02
P3BHT11	10.1	0.068	4.65	3.45	1.15×10^3	3.18
P3BHT12	4.7	0.473	9.70	2.32	0.96×10^3	1.13
P3HT	10.1	0.027	3.80	2.30	1.52×10^3	3.54

P3BT/$PC_{71}BM$ blend film due to a higher degree of crystalline P3BT (Fig. 3a). The dense P3BT crystalline domains imposed a beneficial impact on the hole mobility as the hole carrier can easily proceed along the ordered crystalline domains at the faster speed with longer lifetime.[16,46] However, the diffusion of $PC_{71}BM$ molecules in the blend film may largely be constrained by the crystalline P3BT domains, thereby suppressing the formation of percolating $PC_{71}BM$ domains.[28] Therefore, the crystallization of P3BT dominated over the $PC_{71}BM$ diffusion, and was responsible for the observed low performance of the P3BT/$PC_{71}BM$ solar cell.

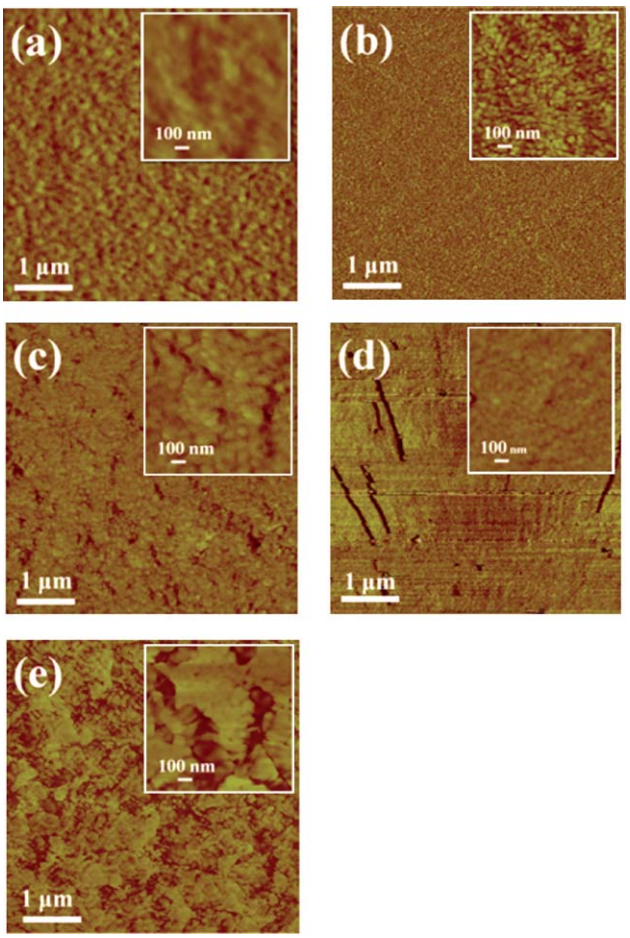

Fig. 3 AFM phase images of blend films: (a) P3BT/$PC_{71}BM$; (b) P3BHT21/$PC_{71}BM$; (c) P3BHT11/$PC_{71}BM$; (d) P3BHT12/$PC_{71}BM$; (e) P3HT/$PC_{71}BM$. All blend films were prepared by following the fabrication procedures of photovoltaic devices but without depositing the Ca/Al layers on the top. The scanning size = 5×5 μm^2 for all images, and 1×1 μm^2 for all insets.

A finer phase separation appeared in the P3BHT21/$PC_{71}BM$ blend film, with dot-like P3BHT21 crystalline domains homogeneously dispersed in the matrix (Fig. 3b), which was indicative of intimate mixing of P3BHT21 and $PC_{71}BM$ at the nanoscale. Compared with P3HT/$PC_{71}BM$ (inset in Fig. 3e), the reduced crystal size and inter-crystal distance in P3BHT21/$PC_{71}BM$ suggested stronger interchain interaction between P3BHT21 chains (inset in Fig. 3b),[47] which was due primarily to the presence of P3BT block in the copolymer that was capable of packing backbones of P3BHT21 closer within the crystalline lamellae. Furthermore, in comparison with P3BT/$PC_{71}BM$ (inset in Fig. 3a), $PC_{71}BM$ appeared to be more uniformly distributed in P3BHT21/$PC_{71}BM$. This implied better diffusion of $PC_{71}BM$ molecules throughout the blend film, which can be ascribed to the presence of P3HT block in the copolymer that rendered the chain flexibility.[2,48] Taken together, the P3BHT21/$PC_{71}BM$ solar cell displaying the highest PCE accompanied by the highest photogenerated charge current, J_L, the lowest ideality factor, n, and the lowest series resistance, r_s (Table 2), was associated with the finer phase separation for charge generation (highest J_L and lowest n) and enhanced crystalline pathway for charge transport (lowest r_s). A similar phase-separated morphology was observed in P3BHT11/$PC_{71}BM$ (inset in Fig. 3c). However, the domains tended to pack denser than those in P3BHT21/$PC_{71}BM$ (*i.e.*, slightly large domain in Fig. 3c), corresponding to a reduced FF in the P3BHT11/$PC_{71}BM$ blend film. The microscopic phase separation[27] was evidenced in P3BHT12/$PC_{71}BM$ as shown in Fig. 3d; such crude phase separation accounted for the lowest J_{sc} and FF among all three P3BHT/$PC_{71}BM$ blend films studied.

The surface roughness of the active layer (*i.e.*, the interface that contacts with the cathode in the resulting solar cell) also has a crucial influence on the PCE. Recently, a root-mean-square (rms) surface roughness of 9.5 nm was reported in the P3HT/PCBM device with the highest PCE of 4.37% by controlling the rate of solvent evaporation.[17] In the present study, the P3BHT21/$PC_{71}BM$, P3BHT11/$PC_{71}BM$, and P3HT/$PC_{71}BM$ blend films showed similar rms surface roughnesses of 8.8 nm, 8.0 nm, and 8.9 nm, respectively (Fig. S1 in the ESI†). While the P3BHT12/$PC_{71}BM$ and P3BT/$PC_{71}BM$ blend films had rather smooth surfaces with rms surface roughnesses of 2.0 nm and 2.9 nm, respectively. So it is clear that a rougher surface could also lead to a better performance in P3BHT/$PC_{71}BM$ BHJ solar cells. It is noteworthy that the rougher surface may not originate from the formation of enhanced ordering of polymer structures (*i.e.*, forming crystals) in the present study, because P3BT showed the highest degree of crystallization as revealed by X-ray diffraction measurement and will be discussed later, and yet had a rather smooth surface (*i.e.*, rms surface roughness of 2.0 nm). Thus, it is plausible that the increase in surface roughness may arise from

the vertical diffusion of $PC_{71}BM$ molecules towards the cathode.[48] More systematic study on the diffusion of $PC_{71}BM$ in the P3BHT system and the effect of surface roughness on the photovoltaic performances is currently underway.

To scrutinize the percolation networks spanning the phase-separated active layer of P3BHT/$PC_{71}BM$, the charge transport was investigated by measuring the space charge limited current (SCLC) hole mobility. In order to fabricate the SCLC hole-only devices, instead of the Ca/Al layer, a thin layer of gold was deposited on the active layer. The hole mobility values were extracted from the current density–voltage (J_{SCLC}–V) curves (Fig. 4) that were fitted by applying the modified Mott–Gurney equation:[49]

$$J_{SCLC} = \frac{9}{8}\varepsilon\varepsilon_0\mu\frac{V^2}{L^2}\exp\left(\frac{0.89\beta}{\sqrt{L}}\sqrt{V}\right) \quad (2)$$

where J_{SCLC} is the dark current density, V is the applied voltage, L is the thickness of active layer, μ is the mobility, ε is the dielectric constant, ε_0 is the permittivity of free space, and β is the field-activation factor.[50] The β values yielded from the P3BT-, P3BHT- and P3HT-based devices were in the range of -4.2×10^{-4} to -8.4×10^{-4} (Table S1 in the ESI†), similar to those reported in P3AT-based devices.[50] Among all five blends, the P3BHT21/$PC_{71}BM$ demonstrated the highest hole mobility of 2.0×10^{-4} cm^2 V^{-1} s^{-1}, correlating very well with the finer nanoscale phase separation observed by AFM (Fig. 3b) and the lowest series resistance derived ($r_s = 1.91$ Ω cm^2 in Table 2). The relatively decreased hole mobility in P3HT/$PC_{71}BM$ and P3BT/$PC_{71}BM$ blends was indicative of increased recombination during the charge transport. Combined with the above film morphology study, the highest hole mobility in P3BHT21/$PC_{71}BM$ apparently resulted from the finer phase separation between P3BHT21 and $PC_{71}BM$ as well as the sufficient P3BHT21 crystal-composed continuous pathway from top to bottom electrodes, reflecting on enhanced J_{sc} and PCE in the P3BHT21/$PC_{71}BM$ BHJ solar cell.[14]

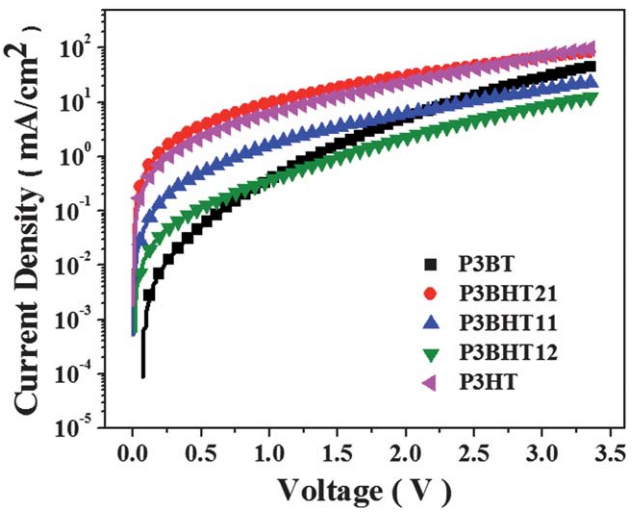

Fig. 4 J–V curves of the space-charge limited current (SCLC) devices for measuring the hole mobility in P3BT/$PC_{71}BM$, P3BHT/$PC_{71}BM$, and P3HT/$PC_{71}BM$ blend films. The SCLC devices were produced by following the fabrication procedures of photovoltaic devices, but depositing the gold layer on the top of active layers instead of the Ca/Al layers. The symbols are experimental data, while the solid lines are the corresponding theoretical fits.

3.4. Molecular organization of P3BHT/$PC_{71}BM$ blend films

The molecular organization of P3BHT in the blend films was elucidated by X-ray diffraction (XRD) measurements in Fig. 5. The XRD profiles of P3BT and P3HT in the corresponding blend films were also measured and compared with that of P3BHT; these provided insight into the influence of different alkyl side chains on the structural ordering and orientation of P3BHT chains. Compared with the XRD profiles of pristine P3BT, P3HT and P3BHT films without blending with $PC_{71}BM$ (Fig. 1b), no significant changes in the shape and peak position of the XRD profiles were observed, indicating that P3BHT chains in the blend films retained their molecular organization in the pristine films, where P3BT and P3HT blocks co-crystallized into a lamellar packing with the tunable interchain distance along the (100) axis as illustrated in Fig. 1c. The co-crystalline P3BHT domains formed microphase separation with $PC_{71}BM$ domains as shown in Fig. 3, which is intrinsically varied with the molecular packing of P3BHT chains and the diffusion of $PC_{71}BM$ molecules in the blend.[27,48]

Considering the thicknesses of all blend films are approximately 200 nm, the intensity of the [100] peak was nearly proportional to the size or the number of polymer crystals per unit volume in the blend films. In addition to the higher degree of crystallinity of P3AT that is correlated with enhanced light absorption and increased hole mobility, other factors such as the phase separation in the active layer, the interpenetrating network of each separated phase, and the size of P3AT crystalline domains would also affect the ultimate device performance.[48,51] For efficient charge generation without significant recombination, the size of crystalline P3AT domain should be comparable to or less than the exciton diffusion length (often in the range of 10 nm).[52] P3BT showed the highest crystallinity as evidenced by the strongest intensity of the [100] peak at $2\theta = 6.7°$ (Fig. 5a). However, the size of P3BT crystals was about 22.7 nm calculated

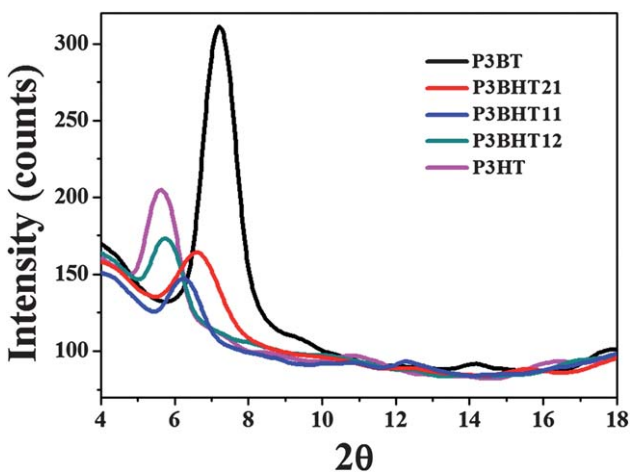

Fig. 5 XRD profiles of P3BT/$PC_{71}BM$, P3BHT/$PC_{71}BM$, and P3HT/$PC_{71}BM$ blend films prepared by following the fabrication procedures of photovoltaic devices, but without depositing the Ca/Al layers on the top.

from the full width at half-maximum (FWHM) of the diffraction peak. Such large size prevented efficient exciton diffusion to the P3BT/$PC_{71}BM$ interface, thereby accounting for the low photogenerated charge density in P3BT/$PC_{71}BM$. The average size of crystalline P3HT domain was 14.4 nm, in good agreement with typical values of 12–16 nm reported in the literature.[53] The smallest domain size of 10.4 nm was achieved in the P3BHT21/$PC_{71}BM$ system, coincided very well with the dot-like P3BHT21 crystalline domains observed in the AFM phase image (Fig. 3b). Thus, in the P3BHT21/$PC_{71}BM$ solar cell, the exciton generated in the crystalline P3HT domain could effectively diffuse to the P3BHT21/$PC_{71}BM$ interface. Additionally, the smaller crystalline domain provided more interface for charge separation (*i.e.*, exciton dissociation). Finally, the closer packing of P3BHT21 chains along the alkyl side chain direction also facilitated the charge transport from interfaces to electrodes.[52,54]

To further resolve the molecular organization of P3AT chains, UV-Vis absorption measurements were performed based on the intermolecular coupling induced absorption shift and intensity variation in the spectra.[55] The absorption spectra of P3BT and P3HT in the blend films were similar to each other, with three peaks at wavelengths, λ, of 530 nm, 557 nm, and 606 nm as shown in Fig. 6a. As the thicknesses of the blend films were the same, the highest absorption intensity of P3BT corresponded very well to the highest degree of P3BT crystallization measured by XRD (Fig. 5a).[51] Notably, compared to P3BT and P3HT, the λ of three absorption maxima in three P3BHT in the blends (P3BHT12, P3BHT11, and P3BHT21) slightly blue-shifted to 505 nm, 552 nm, and 601 nm, respectively. The blue-shift may be attributed to the reduced interchain interactions due to the disruption by adjacent $PC_{71}BM$ molecules, indicating that more $PC_{71}BM$ molecules may disperse between the crystalline P3BHT domains.[56] Such disruption appeared to be advantageous in P3BHT21/$PC_{71}BM$ and P3BHT11/$PC_{71}BM$ blends in which well-defined nanoscale phase separation (Fig. 3b and 2c) and small crystalline size around 10 nm (Fig. 5) were observed. However, the disruption seemed to be unfavorable in the P3BHT12/$PC_{71}BM$ blend film in which the ordered π–π stacking structures were seriously perturbed by $PC_{71}BM$ molecules, representing a microscopic phase separation (Fig. 3d) and the dramatically decreased intensity at $\lambda = 601$ nm that is associated with the degree of π-stacked thienyl backbones.[28,48]

The external quantum efficiency (EQE) of the BHJ solar cells was also measured (Fig. 6b), which provides information on the current obtained outside the device per incoming photon.[14] The maximum EQE of P3BT/$PC_{71}BM$ was nearly 24%, due to the mismatch between the ordered stacking of P3BT chains and the diffusion of $PC_{71}BM$ molecules in the blend films (black curve in Fig. 6b). The short butyl side chain favored the self-assembly of P3BT chains, but lacked enough flexibility to yield well-defined phase separation. The improved balance can, however, be realized in P3HT/$PC_{71}BM$ by increasing the length of side chain to hexyl (pink curve in Fig. 6b). It is interesting to note that the EQE of the device fabricated with P3HT was significantly lower than that fabricated with P3BHT21 (red curve in Fig. 6b) at the wavelength below 450 nm, while the EQE was the same at longer wavelength. It has demonstrated that incomplete exciton harvesting in large fullerene domains can lead to low quantum efficiency at the wavelength below 450 nm as fullerenes absorbed

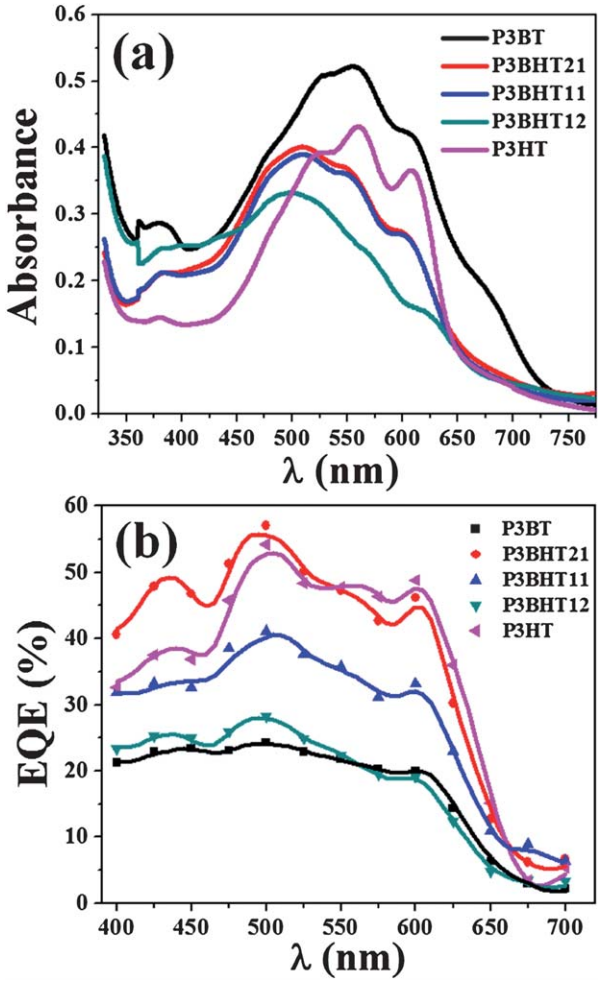

Fig. 6 (a) UV-Vis spectra of P3BT/$PC_{71}BM$, P3BHT/$PC_{71}BM$, and P3HT/$PC_{71}BM$ blend films produced by following the fabrication procedures of photovoltaic devices, but without depositing the Ca/Al layers on the top. (b) EQE spectra of P3BT/$PC_{71}BM$, P3BHT/$PC_{71}BM$, and P3HT/$PC_{71}BM$ blend films obtained directly from the photovoltaic devices.

largely in this wavelength range,[57] which provides further support that P3BHT21 reduced the size of fullerene domains in light of the XRD and AFM results. In this work, the self-assembly and chain flexibility were precisely tailored by capitalizing on P3BHT diblock copolymers *via* varying the composition ratio of P3BT block to P3HT block to accomplish better balance between phase separation for charge generation and interpenetrating, ordered crystalline domains for charge transport and collection. As such, the highest EQE near 60% was obtained in a P3BHT21/$PC_{71}BM$ device (red curve in Fig. 6b).

4. Conclusion

In conclusion, compared to P3AT homopolymer counterparts, better optimized polymer BHJ nanostructures were achieved, *for the first time*, in P3AT rod–rod diblock copolymer-based photovoltaic devices by tuning the ratio of two dissimilar blocks (*i.e.*, P3BT : P3HT = 2 : 1 (mol/mol) in P3BHT21 diblock copolymer). An attractive PCE of 4.02% was yielded in the

P3BHT21/$PC_{71}BM$ photovoltaic device, which was a direct consequence of (1) the formation of small crystalline domains of 10.4 nm that is comparable to the exciton diffusion length in P3ATs, (2) finer phase separation on the nanoscale with a homogeneous P3BHT21/$PC_{71}BM$ interface to maximize the charge generation, and (3) percolation networks with a hole mobility of 2.0×10^{-4} cm^2 V^{-1} s^{-1} for the charge transport and collection. The effect of the ratio of P3BT block to P3HT block in P3BHT on the molecular organization as well as the morphology of P3BHT/$PC_{71}BM$ blend films that are responsible for the ultimate device performance was scrutinized. The strategy of precisely controlling the ratio of the blocks in all-conjugated block copolymer to yield improved photovoltaic performance may provide insight into many aspects of solar energy conversion, from rational design and synthesis of new materials to engineering of high-efficiency polymer BHJ solar cells.

Acknowledgements

We gratefully acknowledge support from the National Science Foundation (NSF-CBET 0824361). F.Q. acknowledges the support from the National Natural Science Foundation of China (Grant No. 20990231).

Notes and references

1 B. C. Thompson and J. M. J. Frechet, *Angew. Chem., Int. Ed.*, 2008, **47**, 58.
2 L. M. Chen, Z. R. Hong, G. Li and Y. Yang, *Adv. Mater.*, 2009, **21**, 1434.
3 W. U. Huynh, J. J. Dittmer and A. P. Alivisatos, *Science*, 2002, **295**, 2425.
4 J. Y. Kim, K. Lee, N. E. Coates, D. Moses, T. Q. Nguyen, M. Dante and A. J. Heeger, *Science*, 2007, **317**, 222.
5 J. Xu, J. Wang, M. Mitchell, P. Mukherjee, M. Jeffries-El, J. W. Petrich and Z. Q. Lin, *J. Am. Chem. Soc.*, 2007, **129**, 12828.
6 Z. Q. Lin, *Chem.–Eur. J.*, 2008, **14**, 6294.
7 M. D. Goodman, J. Xu, J. Wang and Z. Q. Lin, *Chem. Mater.*, 2009, **21**, 934.
8 M. Byun, R. L. Laskowski, M. He, F. Qiu, M. Jeffries-El and Z. Q. Lin, *Soft Matter*, 2009, **5**, 1583.
9 Y. Liang, Z. Xu, J. Xia, S. T. Tasi, Y. Wu, G. Li, C. Ray and L. Yu, *Adv. Mater.*, 2010, **22**, E135.
10 M. C. Scharber, D. Wuhlbacher, M. Koppe, P. Denk, C. Waldauf, A. J. Heeger and C. L. Brabec, *Adv. Mater.*, 2006, **18**, 789.
11 G. Dennler, M. C. Scharber, T. Ameri, P. Denk, K. Forberich, C. Waldauf and C. J. Brabec, *Adv. Mater.*, 2008, **20**, 579.
12 U. Scherf, A. Gutacker and N. Koenen, *Acc. Chem. Res.*, 2008, **41**, 1086.
13 B. H. Hamadani, S. Y. Jung, P. M. Haney, L. J. Richter and N. B. Zhitenev, *Nano Lett.*, 2010, **10**, 1611.
14 B. Friedel, C. R. McNeill and N. C. Greenham, *Chem. Mater.*, 2010, **22**, 3389.
15 W. L. Ma, C. Y. Yang, X. Gong, K. Lee and A. J. Heeger, *Adv. Funct. Mater.*, 2005, **15**, 1617.
16 V. D. Mihailetchi, H. X. Xie, B. de Boer, L. J. A. Koster and P. W. M. Blom, *Adv. Funct. Mater.*, 2006, **16**, 699.
17 G. Li, V. Shrotriya, J. S. Huang, Y. Yao, T. Moriarty, K. Emery and Y. Yang, *Nat. Mater.*, 2005, **4**, 864.
18 H. W. Tang, G. H. Lu, L. G. Li, J. Li, Y. Z. Wang and X. N. Yang, *J. Mater. Chem.*, 2010, **20**, 683.
19 F. C. Chen, C. J. Ko, J. L. Wu and W. C. Chen, *Sol. Energy Mater. Sol. Cells*, 2010, **94**, 2426.
20 V. Shrotriya, Y. Yao, G. Li and Y. Yang, *Appl. Phys. Lett.*, 2006, **89**, 063505.
21 J. Peet, M. L. Senatore, A. J. Heeger and G. C. Bazan, *Adv. Mater.*, 2009, **21**, 1521.
22 G. K. Mor, S. Kim, M. Paulose, O. K. Varghese, K. Shankar, J. Basham and C. A. Grimes, *Nano Lett.*, 2009, **9**, 4250.
23 C. S. Kim, L. L. Tinker, B. F. DiSalle, E. D. Gomez, S. Lee, S. Bernhard and Y. L. Loo, *Adv. Mater.*, 2009, **21**, 3110.
24 H. H. Liao, L. M. Chen, Z. Xu, G. Li and Y. Yang, *Appl. Phys. Lett.*, 2008, **92**, 173307.
25 F. C. Chen, J. L. Wu and Y. Hung, *Appl. Phys. Lett.*, 2010, **96**, 193304.
26 F. C. Chen, J. L. Wu, C. L. Lee, W. C. Huang, H. M. P. Chen and W. C. Chen, *IEEE Electron Device Lett.*, 2009, **30**, 727.
27 G. Q. Ren, P. T. Wu and S. A. Jenekhe, *Chem. Mater.*, 2010, **22**, 2020.
28 H. Xin, G. Q. Ren, F. S. Kim and S. A. Jenekhe, *Chem. Mater.*, 2008, **20**, 6199.
29 P. T. Wu, G. Q. Ren, C. X. Li, R. Mezzenga and S. A. Jenekhe, *Macromolecules*, 2009, **42**, 2317.
30 R. S. Loewe, S. M. Khersonsky and R. D. McCullough, *Adv. Mater.*, 1999, **11**, 250.
31 J. Ge, M. He, F. Qiu and Y. L. Yang, *Macromolecules*, 2010, **43**, 6422.
32 M. He, J. Ge, M. Fang, F. Qiu and Y. L. Yang, *Polymer*, 2010, **51**, 2236.
33 M. He, L. Zhao, J. Wang, W. Han, Y. L. Yang, F. Qiu and Z. Q. Lin, *ACS Nano*, 2010, **4**, 3241.
34 G. H. Lu, L. G. Li and X. N. Yang, *Adv. Mater.*, 2007, **19**, 3594.
35 P. T. Wu, G. Q. Ren and S. A. Jenekhe, *Macromolecules*, 2010, **43**, 3306.
36 A. Salleo, R. J. Kline, D. M. DeLongchamp and M. L. Chabinyc, *Adv. Mater.*, 2010, **22**, 3812.
37 S. S. van Bavel, M. Barenklau, G. de With, H. Hoppe and J. Loos, *Adv. Funct. Mater.*, 2010, **20**, 1458.
38 A. Gadisa, W. D. Oosterbaan, K. Vandewal, J. C. Bolsee, S. Bertho, J. D'Haen, L. Lutsen, D. Vanderzande and J. V. Manca, *Adv. Funct. Mater.*, 2009, **19**, 3300.
39 C. Piliego, T. W. Holcombe, J. D. Douglas, C. H. Woo, P. M. Beaujuge and J. M. J. Frechet, *J. Am. Chem. Soc.*, 2010, **132**, 7595.
40 C. Y. Liu, Z. C. Holman and U. R. Kortshagen, *Adv. Funct. Mater.*, 2010, **20**, 2157.
41 S. H. Park, A. Roy, S. Beaupre, S. Cho, N. Coates, J. S. Moon, D. Moses, M. Leclerc, K. Lee and A. J. Heeger, *Nat. Photonics*, 2009, **3**, 297.
42 C. Waldauff, P. Schilinsky, J. Hauch and C. J. Brabec, *Thin Solid Films*, 2004, **451–52**, 503.
43 C. Waldauf, M. C. Scharber, P. Schilinsky, J. A. Hauch and C. J. Brabec, *J. Appl. Phys.*, 2006, **99**, 104503.
44 P. Schilinsky, C. Waldauf, J. Hauch and C. J. Brabec, *J. Appl. Phys.*, 2004, **95**, 2816.
45 A. Kumar, R. Devine, C. Mayberry, B. Lei, G. Li and Y. Yang, *Adv. Funct. Mater.*, 2010, **20**, 2729.
46 P. Pingel, A. Zen, R. D. Abellon, F. C. Grozema, L. D. A. Siebbeles and D. Neher, *Adv. Funct. Mater.*, 2010, **20**, 2286.
47 G. Li, V. Shrotriya, Y. Yao, J. S. Huang and Y. Yang, *J. Mater. Chem.*, 2007, **17**, 3126.
48 M. Campoy-Quiles, T. Ferenczi, T. Agostinelli, P. G. Etchegoin, Y. Kim, T. D. Anthopoulos, P. N. Stavrinou, D. D. C. Bradley and J. Nelson, *Nat. Mater.*, 2008, **7**, 158.
49 P. n. Murgatro, *J. Phys. D: Appl. Phys.*, 1970, **3**, 151.
50 H. Xin, X. G. Guo, F. S. Kim, G. Q. Ren, M. D. Watson and S. A. Jenekhe, *J. Mater. Chem.*, 2009, **19**, 5303.
51 T. J. Savenije, J. E. Kroeze, X. N. Yang and J. Loos, *Adv. Funct. Mater.*, 2005, **15**, 1260.
52 J. M. Guo, H. Ohkita, H. Benten and S. Ito, *J. Am. Chem. Soc.*, 2010, **132**, 6154.
53 D. E. Motaung, G. F. Malgas, C. J. Arendse, S. E. Mavundla, C. J. Oliphant and D. Knoesen, *J. Mater. Sci.*, 2009, **44**, 3192.
54 J. M. Guo, H. Ohkita, S. Yokoya, H. Benten and S. Ito, *J. Am. Chem. Soc.*, 2010, **132**, 9631.
55 E. Collini and G. D. Scholes, *Science*, 2009, **323**, 369.
56 G. Li, Y. Yao, H. Yang, V. Shrotriya, G. Yang and Y. Yang, *Adv. Funct. Mater.*, 2007, **17**, 1636.
57 G. F. Burkhard, E. T. Hoke, S. R. Scully and M. D. McGehee, *Nano Lett.*, 2009, **9**, 4037.

